CHAPTER IV
RESULTS AND DISCUSSION

4.1 Characterization of Fresh Catalysts

Table 4.1 shows the designed composition of mono- and bimetallic catalysts prepared in this works. The monometallic catalysts (Pt/KL, Sn/KL, and Ge/KL) and bimetallic catalysts (PtSn/KL and PtGe/KL) were prepared by vapor-phase impregnation and vapor-phase co-impregnation, respectively. In general, the catalysts prepared by this technique contain same amount of metal that was added in the catalyst preparation. Therefore, the composition of catalyst in Table 4.1 is reported as the designed composition, which corresponds to the real composition.

Table 4.1 Composition of the catalysts

Catalyst	Composition (wt%)			Mole ratio of Promoter:Pt
	Pt	Sn	Ge	
0.6Pt/KL	0.6	0	0	-
1Sn/KL	0	1.0	0	-
1Ge/KL	0	0	1.0	-
0.6Pt0.6Sn/KL	0.6	0.6	0	1.64
0.6Pt0.3Ge/KL	0.6	0	0.3	1.34
0.6Pt0.6Ge/KL	0.6	0	0.6	2.69
0.6Pt1Ge/KL	0.6	0	1.0	4.48
0.6Pt3Ge/KL	0.6	0	3.0	13.44

To investigate the reducibility of catalysts, the Pt/KL, Pt–Sn/KL, and Pt–Ge/KL catalysts were characterized by TPR. Figure 4.1 shows the TPR profiles of the mono- and bimetallic catalysts supported on commercial KL zeolite. For the monometallic Pt catalyst, a main reduction peak centered at 210 °C which is attributed to the reduction of Pt^{2+} in the main channels. The peak at 450 °C was denoted for the reduction of Pt^{2+} in hidden sites of L zeolite (Zheng *et al.*, 1996). On the contrary, the TPR profile of Sn consists of one broad peak from 350 to 550 °C

(Trakarnroek *et al.*, 2007). Besides, the reduction of Ge exhibited two small peaks at 460 °C and 620 °C, and one large peak at 720 °C. For bimetallic catalysts, PtSn/KL catalyst presents one broad reduction peak which did not match with the combined profile of monometallic Pt and Sn catalysts. It could be assigned to the formation of Pt–Sn alloy phase. Whereas the reduction profile of PtGe/KL showed large fractions of Pt-rich phase and Ge-rich phase, however, the second peak of Pt shifts to a higher temperature which indicated some interaction of Pt and Ge. The TPR profiles of bimetallic PtGe/KL catalysts with various amounts of germanium loading, i.e., 0.6Pt0.3Ge, 0.6Pt0.6Ge, 0.6Pt1Ge, and 0.6Pt3Ge, revealed such an interaction as shown in Figure 4.2.

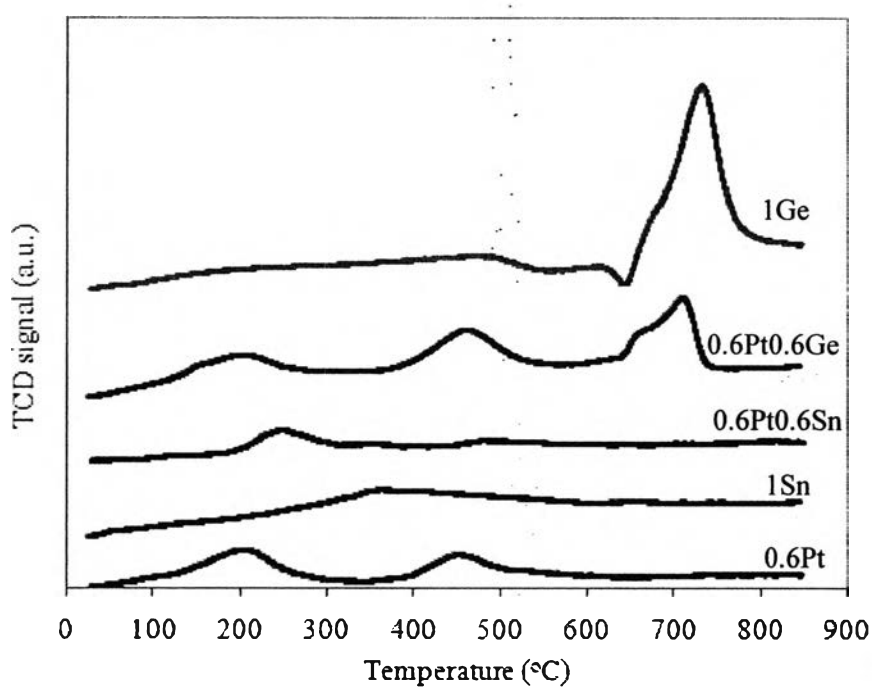

Figure 4.1 TPR profiles of the mono- and bimetallic catalysts prepared by vapor-phase impregnation method.

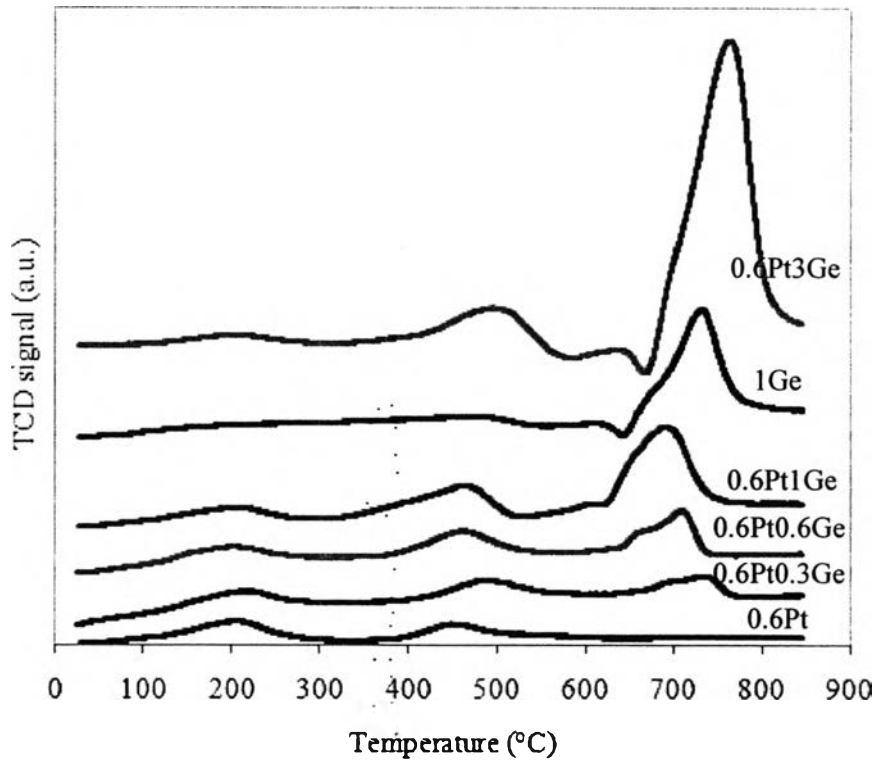

Figure 4.2 TPR profiles of the bimetallic Pt–Ge catalysts with various amounts of germanium loading prepared by vapor-phase impregnation method.

TEM images of the Pt, Pt-Sn, and Pt-Ge catalysts are illustrated in Figure 4.3. Pt particles outside the zeolite were detected. The results showed that the addition of tin and germanium enhanced the dispersion of the metals and also decreased the particle size of the metals when compared with those of the unpromoted Pt/KL catalyst. For the Pt-Ge catalyst with different Ge loading, it was apparent that 0.6Pt0.6Ge showed the smallest the particle size of the metals. Besides, the results of EDX illustrated that Sn element was close to Pt element as shown in Figure 4.4. Thus, it might be proposed that Pt and Sn are in alloy form. In contrast, there is no Ge element residing nearby Pt and there is no Pt element residing nearby Ge. This evidence indicates that Pt and Ge do not form alloy.

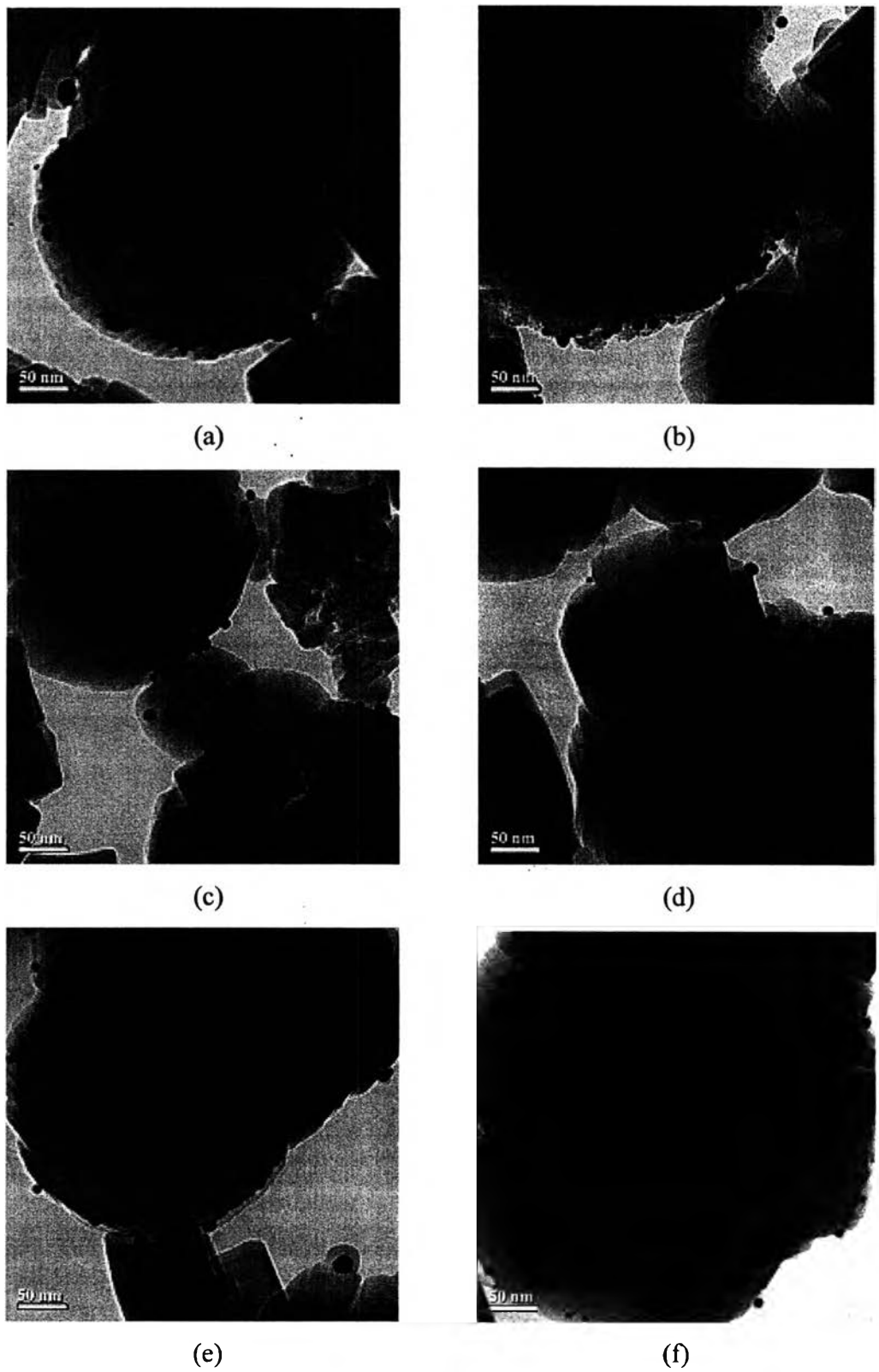

Figure 4.3 TEM images of the monometallic (a) 0.6Pt/KL and bimetallic (b) 0.6Pt0.6Sn/KL, (c) 0.6Pt0.3Ge/KL, (d) 0.6Pt0.6Ge/KL , (e) 0.6Pt1Ge/KL, (f) 0.6Pt3/KL catalysts.

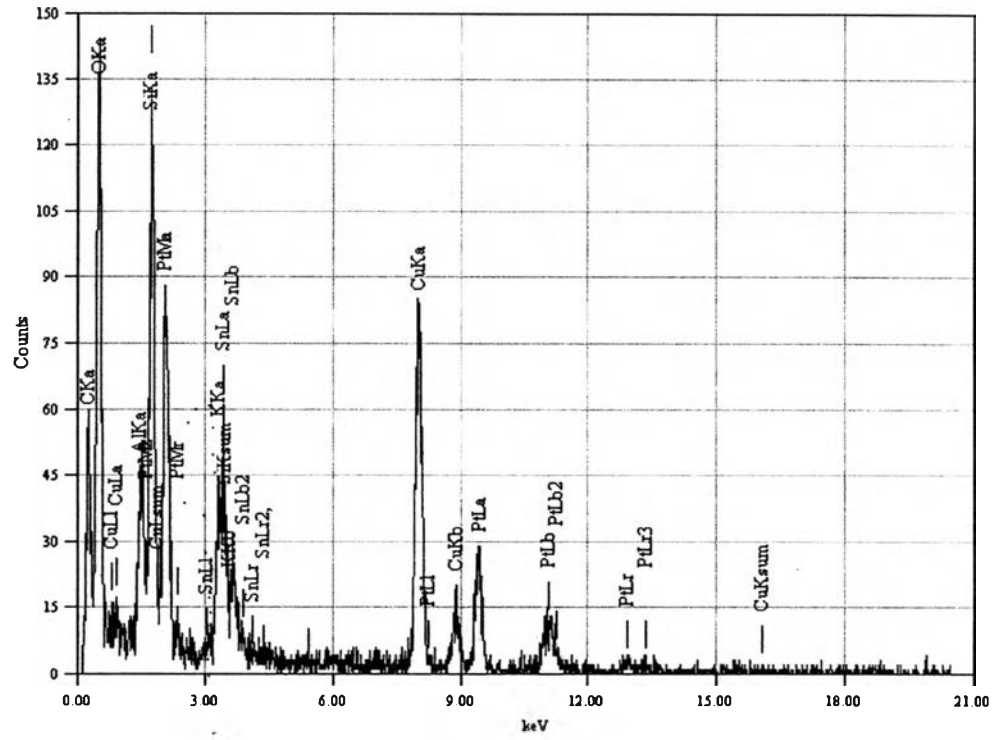

(a)

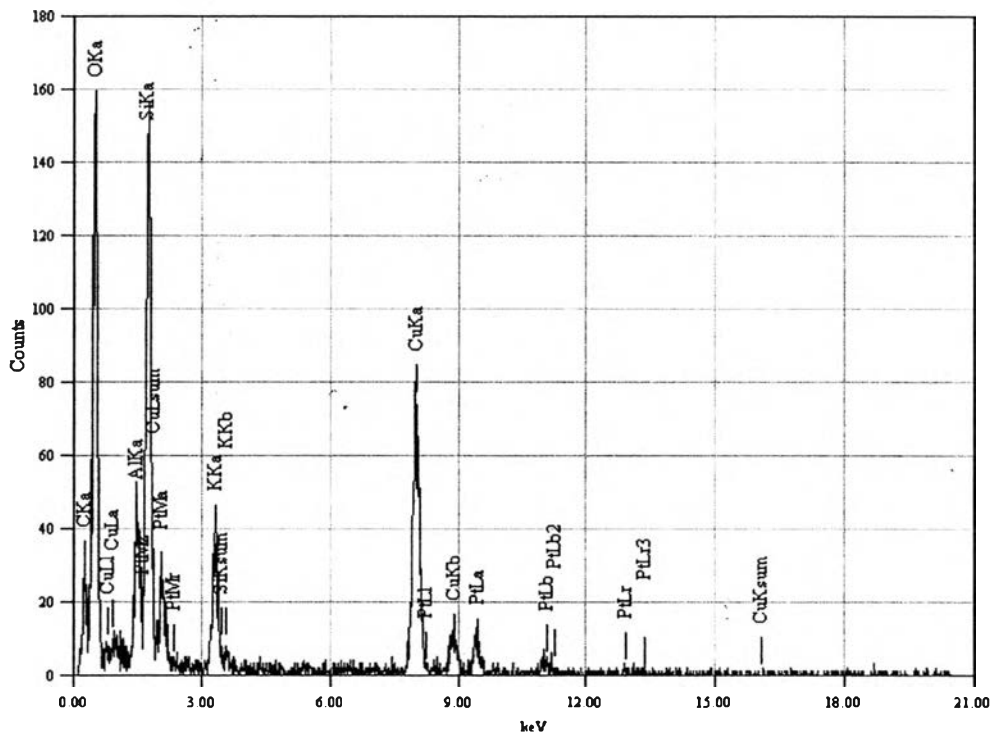

(b)

Figure 4.4 EDX profiles of the bimetallic (a) 0.6Pt0.6Sn/KL, (b) 0.6Pt0.6Ge/KL (Pt rich), and (c) 0.6Pt0.6Ge/KL (Ge rich) catalysts.

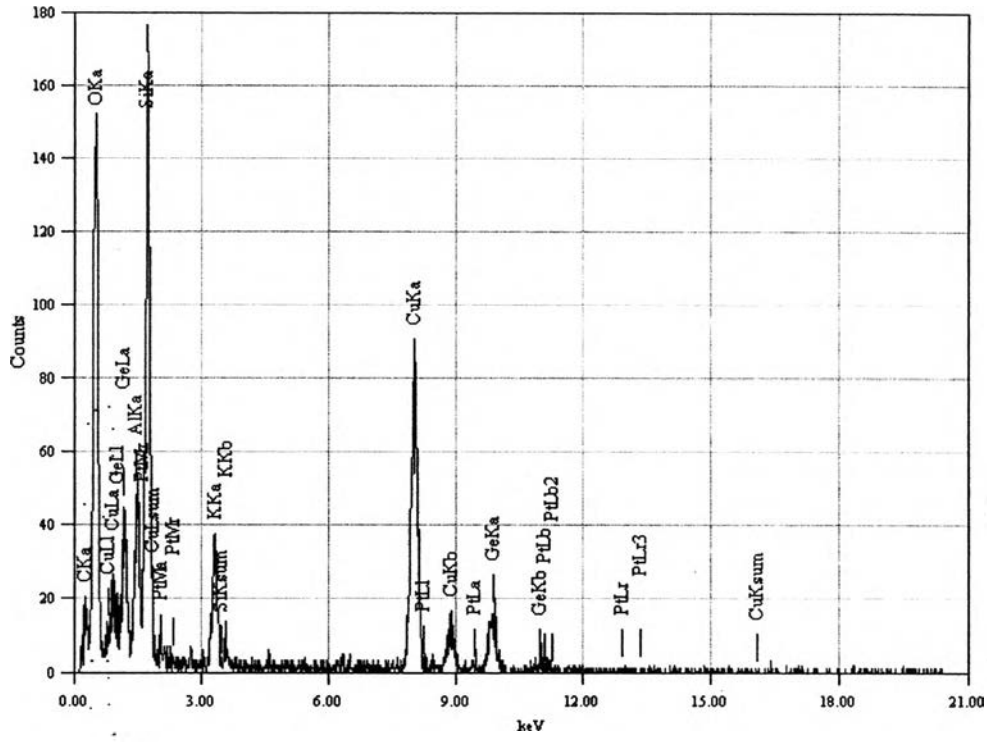

(c)

Figure 4.4 (Continued) EDX profiles of the bimetallic (a) 0.6Pt0.6Sn/KL, (b) 0.6Pt0.6Ge/KL (Pt rich), and (c) 0.6Pt0.6Ge/KL (Ge rich) catalysts.

The results of hydrogen chemisorption are also reported in Table 4.2. The unpromoted Pt catalyst exhibited higher H/Pt ratio than the promoted Pt-Sn and Pt-Ge catalysts. This implied that the addition of tin and germanium elements, which did not chemisorb hydrogen, causes a strong decrease in the H/Pt ratio because Sn and Ge may modify its electronic property resulted in a low hydrogen adsorption (Passos *et al.*, 1998 and Crabb *et al.*, 2001). The change in electronic property of Sn and Ge is discussed in XPS section.

Table 4.2 Hydrogen chemisorption results of the monometallic Pt/KL and bimetallic PtSn/KL and PtGe/KL.

Catalyst	H/Pt ratio after reduction at 500 °C
0.6Pt/KL	0.97
1Sn/KL	0
1Ge/KL	0
0.6Pt0.6Sn/KL	0.29
0.6Pt0.3Ge/KL	0.30
0.6Pt0.6Ge/KL	0.16
0.6Pt1Ge/KL	0.06
0.6Pt3Ge/KL	0.01

The DRIFTS measurements of adsorbed CO on Pt/KL, PtSn/KL, and PtGe/KL catalysts are shown in Figure 4.5. Based on the previous study (Jacobs *et al.*, 2000), the wavenumber bands below 2050 cm^{-1} are related to CO adsorbed on highly dispersed Pt inside the channels of the L-zeolite. During CO adsorption Pt carbonyls can be formed which result from a disruption of the Pt clusters by interaction with CO. Thus, these carbonyls can be formed from very small Pt clusters and can only be stabilized inside the zeolite (Stakheev *et al.*, 1995). By contrast, the band at and above 2075 cm^{-1} are indicated to the Pt external to the pores. Lastly, the band between 2050 and 2075 cm^{-1} are related to CO adsorbed on particles near the pore mouth. The majority of the spectrum obtained on the Pt/KL catalyst below 2075 cm^{-1} indicating that the fractions of Pt particles inside the zeolite and near pore mouth were quite large. Since SiO_2 is nonmicroporous structure, FTIR of adsorbed CO on PtSn/SiO_2, which displays a peak at 2060 cm^{-1} (Llorca *et al.*, 1998), was used for indication the location of Pt-Sn in the KL zeolite. The DRIFTS result showed that the frequency of adsorbed CO on the PtSn/KL catalyst exhibited a sharp peak at around 2070 cm^{-1}. This increasing in wavenumbers for linear stretching, when compared with Pt/KL catalyst, could not be attributed to electronic effects but it

could be ascribed to a larger extent of particles in alloy form outside the zeolite. In agreement with this observation, TEM results of PtSn/KL catalyst have showed the high amounts of particles outside the zeolite. Conversely, for the PtGe/KL catalyst, the position of the spectrum of CO adsorbed was similar to Pt/KL catalyst. Hence, the location of the particle was unaffected by the addition of Ge. In Figure 4.6 representative DRIFTS spectra of CO adsorbed on PtGe/KL catalysts in various the amount of germanium loading are shown.

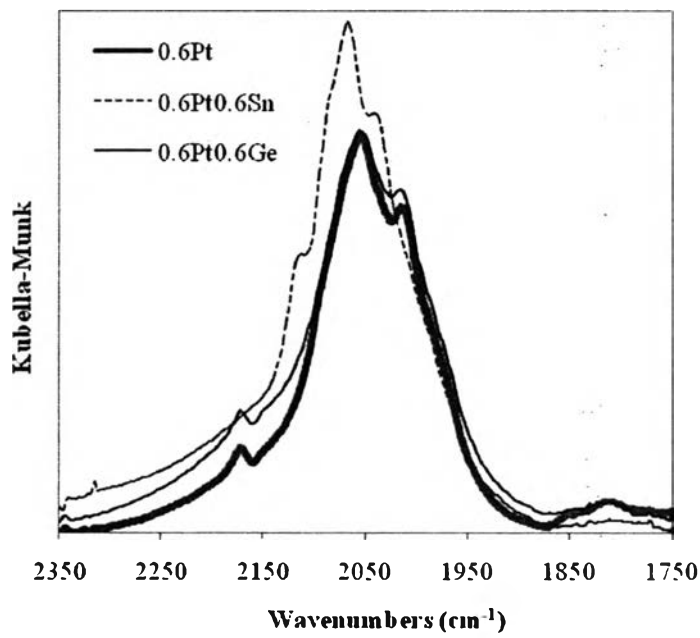

Figure 4.5 DRIFTS spectra of CO adsorbed on Pt/KL, PtSn/KL, and PtGe/KL catalysts reduced in situ at 300 °C. The reduced catalysts were exposed to a flow of 3% CO in He for 30 min at 30 °C and purged in He for 30 min.

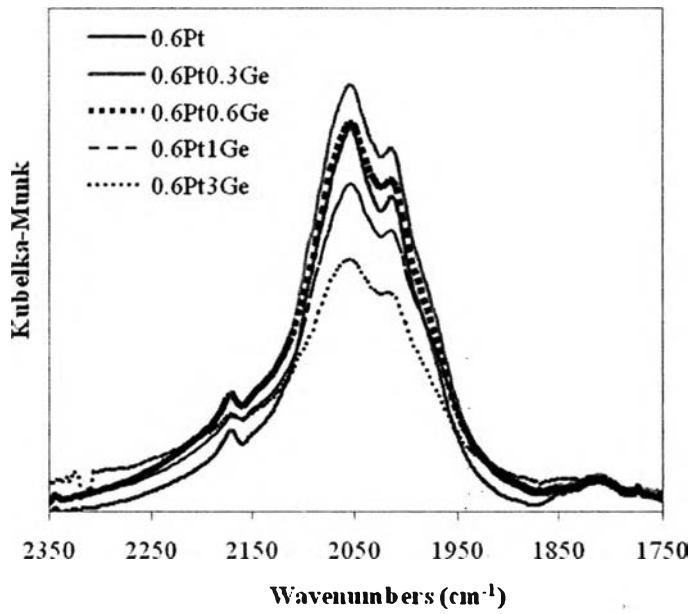

Figure 4.6 DRIFTS spectra of CO adsorbed on PtGe/KL catalysts in various the amount of germanium loading reduced in situ at 300 °C. The reduced catalysts were exposed to a flow of 3% CO in He for 30 min at 30 °C and purged in He for 30 min.

In order to obtain information about the oxidation states of the metal on the surface, X-ray photoelectron spectra of the Sn3d and Ge2p levels were investigated. Figure 4.7 (a) shows the Sn3d XPS spectra of the monometallic 1Sn/KL and bimetallic 0.6Pt0.6Sn/KL catalysts. The peak of metallic tin is found at 484.9 eV, and the peak of tin oxides is present at 486.5 eV (Li *et al.*, 1990). However, it cannot tell the difference between Sn(II) oxide and Sn(IV) oxide from XPS. For the 1Sn/KL XPS spectra, peak was found at 486.5 eV which represented SnO and/or SnO_2. For the 0.6Pt0.6Sn catalyst, Sn3d peak was found at 485 eV which corresponds to Sn^0. Moreover, Sn showed lower binding energy in the presence of Pt. This is because Sn modifies its electronic property by gaining some electron from Pt. Figure 4.7 (b) shows the Ge2p spectrum of the monometallic 1Ge/KL and bimetallic 0.6Pt0.6Ge/KL catalysts. The peak of Ge(II) oxide and Ge(IV) oxide is found at 1220 eV (Briggs *et al.*, 1993). Nevertheless, no Ge^0 is found on the surface of catalysts reduced at 500 °C (Grbic *et al.*, 2006; Arteaga *et al.*, 1999; and Huang *et al.*, 1998). For the reduced 0.6Pt0.6Ge catalyst, the binding energy of the Ge2p

appeared at 1219.5 eV, which can be attributed to Ge^{2+}/Ge^{4+}. It was observed that the XPS spectrum of bimetallic 0.6Pt0.6Ge was shifted toward lower binding energy due to transformation of electrons from Pt to Ge.

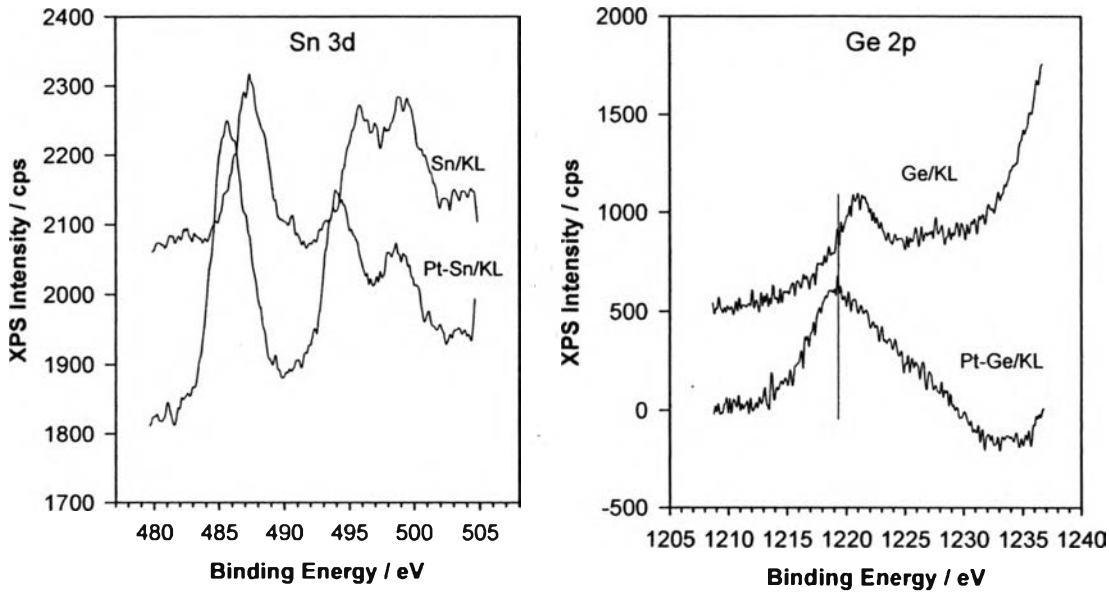

(a) (b)

Figure 4.7 (a) Sn3d XPS spectra of the 1Sn/KL and 0.6Pt0.6Sn/KL catalysts and (b) Ge2p XPS spectra of the 1Ge/KL and 0.6Pt0.6Ge/KL catalysts.

4.2 Catalytic Activity Testing: *n*-Octane Aromatization

4.2.1 Sulfur-free Feed

4.2.1.1 The Effect of Addition of Tin (Sn) and Germanium (Ge

The Pt/KL, PtSn/KL, and PtGe/KL catalysts were tested for *n*-octane aromatization at 500 °C and atmospheric pressure as a function of time on stream. The *n*-octane conversion obtained on mono- and bimetallic catalysts are illustrated in Figure 4.8. It was observed that Pt/KL catalyst exhibits a rapid deactivation due to the restricted diffusion out of the pore of C8-aromatic products (EB and OX) because of coke plugging inside the pores (Jongpatiwut *et al.*, 2005). In previous studies, it was found that the addition of a promoter such as tin and germanium could improve the stability of the catalysts by inhibiting the adsorption of dehydrogenated species which is the intermediate for coke formation (Hill *et al.*, 1998; Cortright *et al.*, 1994, 2000; Borgna *et al.*, 2000).

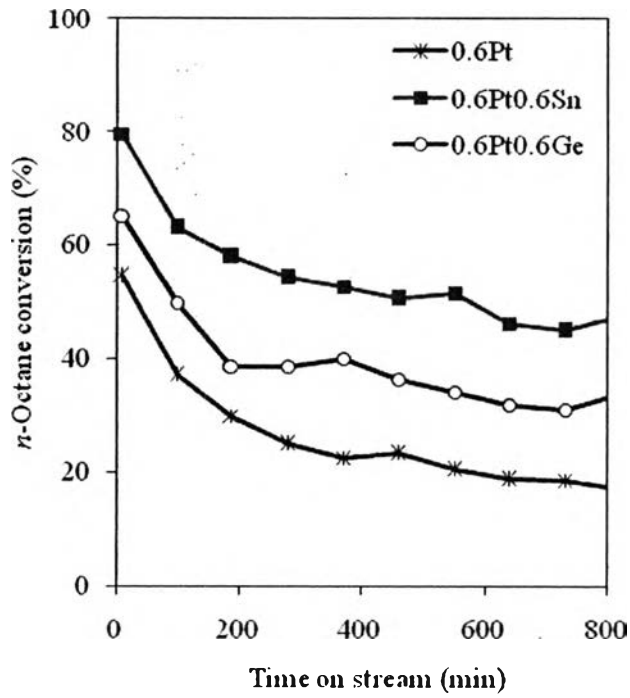

Figure 4.8 The variations of *n*-octane conversion vs. time on stream under *n*-octane clean feed over 0.6Pt/KL, 0.6Pt0.6Sn/KL and 0.6Pt0.6Ge/KL catalysts. Reaction conditions: WHSV = 5 h^{-1}; H_2/HC molar ratio = 6; temperature = 500 °C; pressure = 1 atm.

In terms of product selectivity as shown in Figures 4.9 (a) and 4.9 (b), the results illustrate that PtSn/KL and PtGe/KL yield higher both selectivity to total aromatics and selectivity to C8-aromatics than Pt/KL. As shown in Table 4.3, the major aromatics products on bimetallic PtSn/KL and PtGe/KL catalysts are C8-aromatics (EB and OX) with small amount of benzene and toluene which are undesired products from hydrogenolysis reaction. Therefore, the addition of tin and germanium as a promoter causes a decrease in the hydrogenolysis products and an increase in C8-aromatics products (Trakarnroek *et al.*, 2007). From the results of TEM, it can be suggested that tin and germanium broke the Pt metals into small ensembles. Hence, not only the hydrogenolysis reaction, which requires large ensembles, was decreased by the addition of promoter (Sn or Ge), but the formation of OX molecules was also enhanced as shown in Table 4.3. However, Ge does not help improve the catalytic activity and product selectivity of sulfur-free feed as much as Sn. From TEM results, the size of metal in the presence of Sn is smaller than that of Ge. Therefore, the activity and selectivity to C8-aromatics obtains from 0.6Pt0.6Ge is less than that obtains from 0.6Pt0.6Sn. Based on a previous study, it was notified that the molar ratio of EB/OX may be an indirect index, indicating that electron density of Pt by the addition of Sn (Westfall *et al.*, 1976 and Lee *et al.*, 1994). Davis *et al.* (1969) found that a mechanism to obtain the dehydrocyclization of *n*-octane produced EB and OX involves the direct formation of a six-membered carbon ring. Since the strength of primary hydrogen in $-CH_3$ is only greater than that of secondary hydrogen in $-CH_2$, it was expected that the six-membered ring intermediate would lead to an almost equal amount of EB and OX (Meriaudeau *et al.*, 1997). However, Sn would alter the ability of Pt to rupture the C-H bond and favor the rupture of the weaker C-H bond of the secondary hydrogen of the $-CH_2$ groups over those of the primary hydrogen of the $-CH_3$ groups. Therefore, the EB/OX ratio was decreased when Sn was employed (Trakarnroek *et al.*, 2007). While the EB/OX ratio of 0.6Pt0.6Ge is about unity, which does not improve as much as 0.6Pt0.6Sn. From Table 4.3, it was found that the EB/OX ratio of Pt/KL is higher than that of PtSn/KL and PtGe/KL caused no electrons being transferred from promoter to Pt atoms. Moreover, the EB/OX ratio of Pt greater than unity can be explained in terms of the critical molecule size relative to the zeolite pore size. Since

the critical size of OX molecules is larger than that of EB, the speed of transport through the pores for OX is slower. As a result, OX is highly converted to smaller molecules such as benzene, toluene and methane by secondary hydrogenolysis. However, in this study, the platinum was loaded at 0.6 wt%. This is because M'Kombe *et al.* (1997) found that the 0.6 wt% Pt loading was higher platinum dispersions than 1 wt% Pt loading. Besides, K-zeolite containing 0.6 wt% Pt showed a good correlation between the fineness of the platinum dispersion and *n*-hexane conversion in the aromatization reaction (Fung *et al.*, 1990; McVicker *et al.*, 1993; M'Kombe *et al.*, 1997; and Tauster *et al.*, 1986). In agreement with previous work (Eley *et al.*, 1983), the results showed that the amount of *o*-xylene from *n*-octane conversion increased with decreasing Pt loading of the catalyst as shown in Table 4.3.

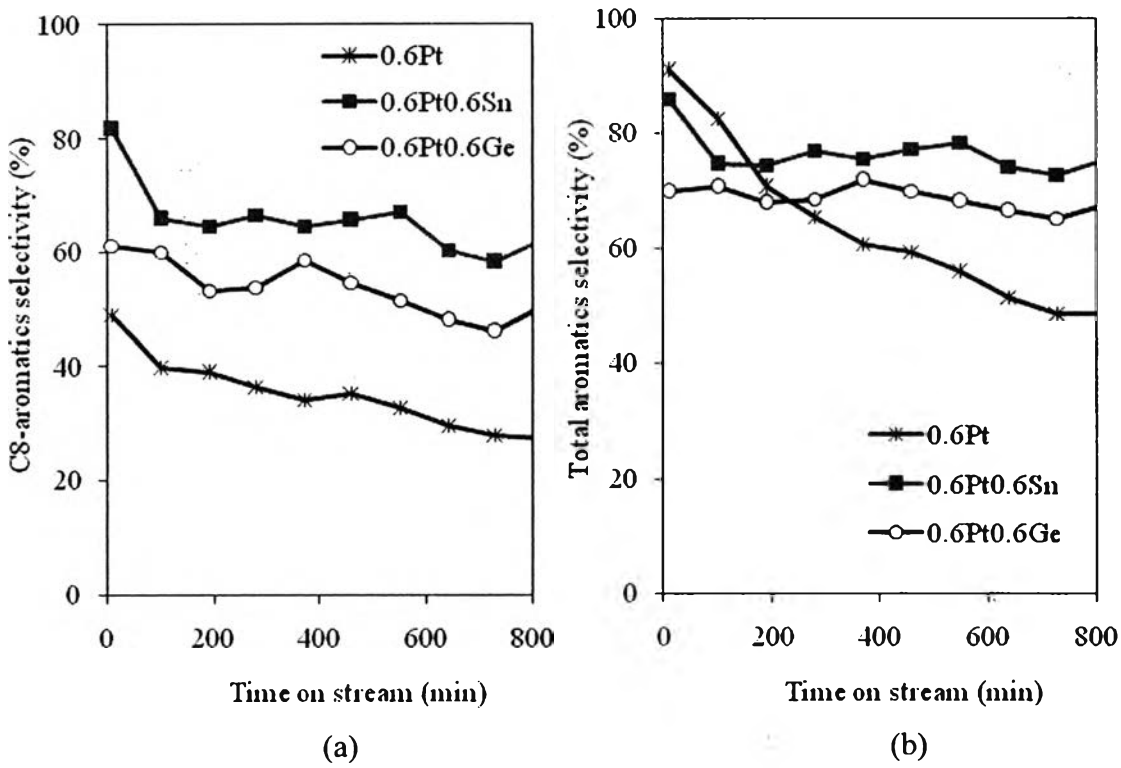

Figure 4.9 The variations of (a) total aromatics selectivity and (b) C8-aromatics selectivity vs. time on stream under *n*-octane clean feed over 0.6Pt/KL, 0.6Pt0.6Sn/KL and 0.6Pt0.6Ge/KL catalysts. Reaction conditions: WHSV = 5 h^{-1}; H_2/HC molar ratio = 6; temperature = 500 °C; pressure = 1 atm.

4.2.1.2 The Effect of Ge loading

To study the effect of Ge loading, 0.6Pt0.3Ge, 0.6Pt0.6Ge, 0.6Pt1Ge, and 0.6Pt3Ge catalysts were prepared. Figure 4.10 shows the *n*-octane conversion for these catalysts as a function of time on stream. The results show that 0.6Pt0.6Ge gave the highest *n*-octane conversion. From TPR results, increasing in the amount of Ge loading led to an increase in Pt–Ge interaction phase. Besides, 0.6 %wt Ge loading showed the smallest metal particle size. Thus, it is apparent that the activity of 0.6Pt0.6Ge was relatively improved via both geometric and electronic effects. However, the activity of the bimetallic PtGe/KL was decreased when the amount of Ge was in excess (> 0.6%wt). As shown in Figure 4.10, the activity of 0.6Pt3Ge is the least since the excess amount of Ge might cover the active sites of Pt.

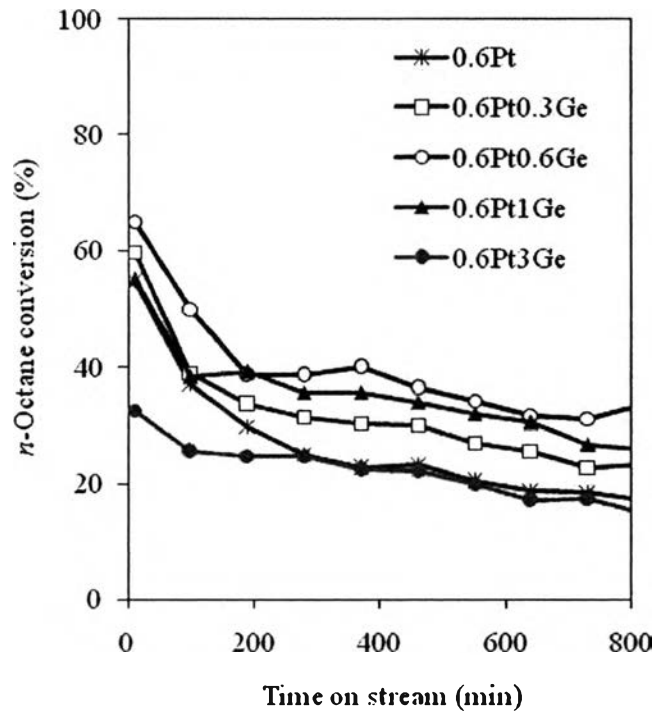

Figure 4.10 The variations of *n*-octane conversion vs. time on stream under *n*-octane clean feed of various Ge loading of the bimetallic PtGe/KL catalysts. Reaction conditions: WHSV = 5 h^{-1}; H_2/HC molar ratio = 6; temperature = 500 °C; pressure = 1 atm.

In terms of product selectivity, the 0.6Pt0.6Ge catalyst exhibits the highest selectivity to total aromatics and C8-aromatics among the Pt/Ge catalysts prepared as shown in Figures 4.11 (a) and 4.11 (b), respectively. The major aromatics products are C8-aromatics. It was observed that the selectivity to total aromatics and C8-aromatics were improved with increasing the amount of Ge loading by geometric and electronic effect. However, they were decreased with an excess amount of Ge. Ge modifies geometric effect by decreased the size of the metal as shown in TEM image. C-C bond hydrogenolysis was inhibited; consequently, the selectivity to benzene was decrease on 0.6Pt0.6Ge as shown in Table 4.3. For electronic effect, the hydrocarbon cannot be strongly adsorbed on the catalyst surface; thus, C-C bond hydrogenolysis was inhibited. In addition, germanium enhanced the ability to break the $-CH_2$ bond. As a result, the EB/OX ratio is decreased as the amount of Ge is increased as shown in Figure 4.12. Nevertheless, the EB/OX ratio was increased when the amount of Ge is higher than 0.6 because this catalyst is less active and selective to aromatic products.

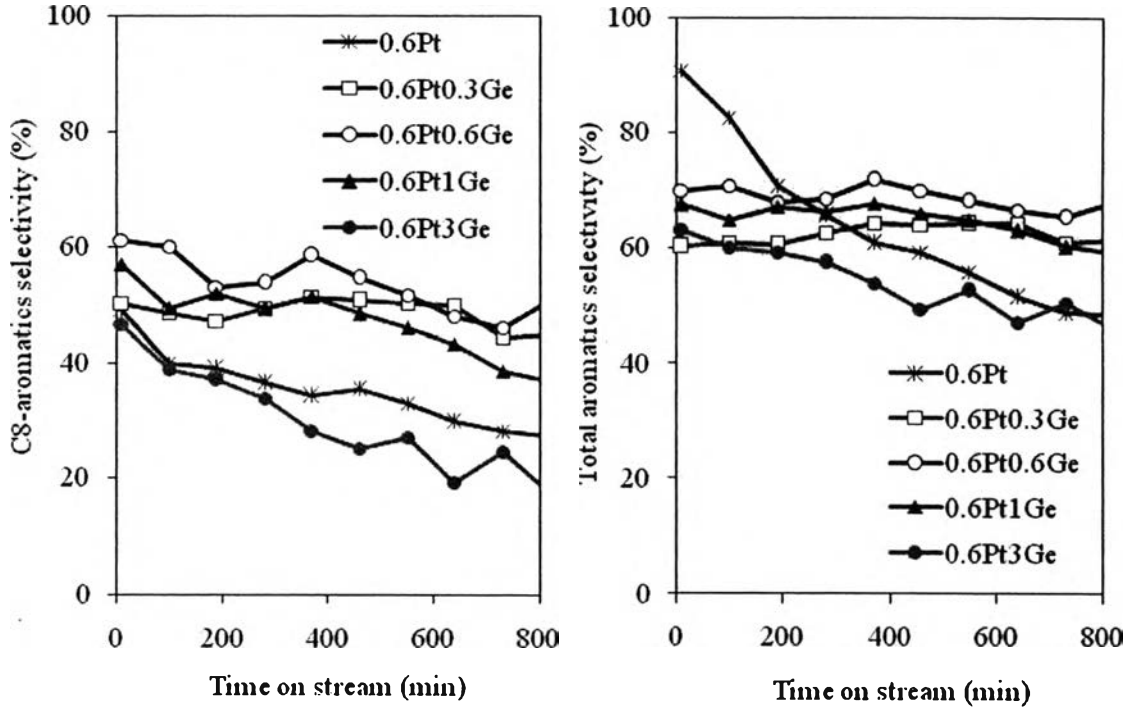

Figure 4.11 The variations of (a) total aromatics selectivity and (b) C8-aromatics selectivity vs. time on stream under *n*-octane clean feed of various Ge loading of the bimetallic PtGe/KL catalysts. Reaction conditions: WHSV = 5 h^{-1}; H_2/HC molar ratio = 6; temperature = 500 °C; pressure = 1 atm.

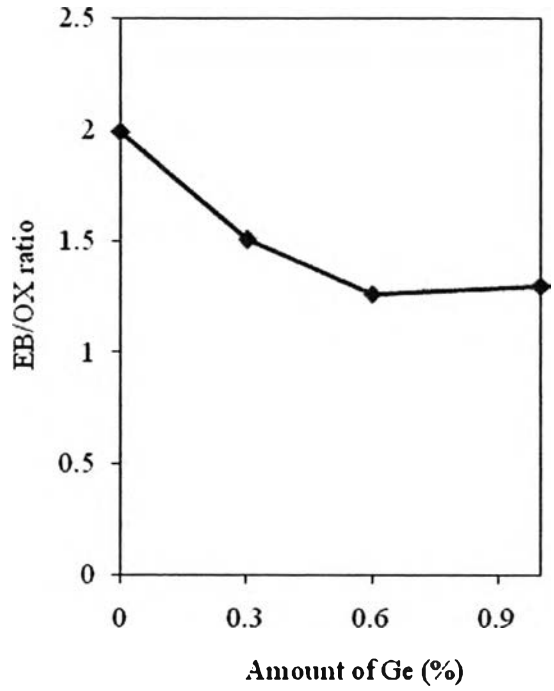

Figure 4.12 The variations of EB/OX ratio at 10 minutes on stream with amount of Ge of the bimetallic PtGe/KL catalysts. Reaction conditions: WHSV = 5 h^{-1}; H_2/HC molar ratio = 6; temperature = 500 °C; pressure = 1 atm.

Table 4.3 Properties of Pt/KL, PtSn/KL, and PtGe/KL catalysts tested for *n*-octane aromatization after 810 minutes on stream under sulfur-free feeds; reaction condition: WHSV = 5 h^{-1}; H_2/HC molar ratio = 6; temperature = 500 °C; pressure = 1 atm

Feed	Sulfur-free feed							Sulfur-containing feed		
Catalyst	1Pt*	0.6Pt	0.6Pt0.6Sn	0.6Pt0.3Ge	0.6Pt0.6Ge	0.6Pt1Ge	0.6Pt3Ge	0.6Pt	0.6Pt0.6Sn	0.6Pt0.6Ge
Conversion (%)	23.28	17.15	47.60	23.28	33.63	25.62	14.80	17.52	65.55	21.30
Product distribution (%)										
C1-C5	19.72	0	0.003	0.16	0.006	0.03	0.03	0.16	0.23	0.03
Total enes (C6-C8enes)	12.40	51.49	24.52	36.63	32.15	40.44	53.97	44.81	18.98	31.37
Total aromatics	67.88	48.51	75.41	61.32	67.77	59.09	45.91	54.80	78.72	67.58
Total aromatics (%)										
Benzene	19.05	0.24	0.14	1.24	0.14	0.20	0.21	0.62	0.64	0.44
Toluene	27.59	21.01	13.01	15.15	16.73	21.99	28.34	23.04	7.95	40.67
C8-aromatics	21.24	27.27	62.26	44.94	50.71	36.89	17.36	31.13	70.13	26.47
EB	13.95	12.86	25.68	21.77	22.36	15.86	7.37	13.74	31.86	10.78
m-, *p*-Xylene	1.82	0.92	4.89	5.78	5.61	5.42	3.35	1.08	0	6.78
o-Xylene	5.47	13.48	31.70	17.39	22.74	15.61	6.64	16.31	38.27	8.90
EB/OX ratio	2.55	0.95	0.81	1.25	0.98	1.02	1.11	0.84	0.83	1.21
Hydrogenolysis products	66.36	21.25	13.15	16.55	17.07	22.22	28.57	23.81	8.82	41.14

*The data were obtained from previous work: Trakarnroek *et al.*, (2007) after 550 minutes on stream.

4.2.2 Sulfur-containing Feed

Sulfur tolerance experiments were performed by adding 25 ppm of sulfur to the feed. The activity under *n*-octane sulfur-containing feed obtained on mono- and bimetallic catalysts are illustrated in Figure 4.13. It was found that the unpromoted Pt/KL catalyst for *n*-octane aromatization was not extremely high sensitivity to sulfur as much as for *n*-hexane aromatization which was found by Jacobs *et al.*, (1998). The sensitivity to sulfur was also found in the aromatization of *n*-octane on Pt-Ge/KL catalyst. Figure 4.14 (a) and (b) show total aromatics selectivity and C8-aromatics selectivity versus time on stream. In the presence of sulfur, Pt-Ge/KL catalyst showed lower C8-aromatics selectivity and higher hydrogenolysis products which are benzene and toluene than clean feed. It probably proposed that the presence of sulfur led to directly weak bonding between metal and support, and then formation of Pt agglomeration which persuaded larger Pt ensembles required for hydrogenolysis reaction. This has to be proved with characterization of the spent catalyst by mild decoking as well as it will be further confirmed by TEM characterization of the spent catalyst. By contrast, on the Pt-Sn/KL catalyst, the *n*-octane aromatization was not only diminished by the addition of sulfur, but also increased. This tolerance can be due to two possible causes: (a) the Sn may prevent Pt growth by acting as anchoring sites for Pt, or (b) Sn may modify electronic effect of the catalyst.

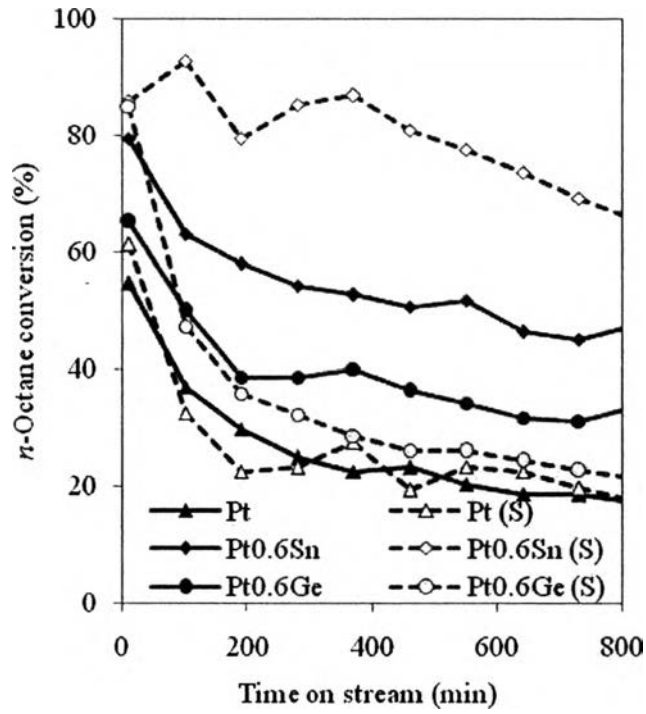

Figure 4.13 The variations of *n*-octane conversion vs. time on stream under 25 ppm sulfur-containing feed over 0.6Pt/KL, 0.6Pt0.6Sn/KL and 0.6Pt0.6Ge/KL catalysts. Reaction conditions: WHSV = 5 h^{-1}; H_2/HC molar ratio = 6; temperature = 500 °C; pressure = 1 atm.

In term of aromatics product selectivity, it was found that benzene selectivity and EB/OX ratio of Pt/KL catalysts in sulfur-containing feed is lower than clean feed as shown in Table 4.3. It would be due to the fact that sulfur made bonding between metal and support weaken and then resulted in the escape of Pt to the outside the zeolite channel (McVicker *et al.*, 1993 and Treacy *et al.*, 1999). As a result, the OX production increased. In addition, in the first 10 minutes, the *n*-octane conversion under 25 ppm sulfur-containing feed over Pt-Ge/KL catalyst was higher than clean feed. It would be because hydrogenolysis reaction is faster than aromatization reaction (Eley *et al.*, 1983). In the case of Pt-Sn/KL catalyst, it is more aromatics selectivity in the presence of sulfur than in the absence of sulfur. As shown in Table 4.3, furthermore, hydrogenolysis was reduced in sulfur-containing feed. This maybe concerns with electronic effect of Sn-promoted catalyst that the

hydrocarbon cannot be strongly adsorbed on the catalyst surface; thus, C-C bond hydrogenolysis was inhibited.

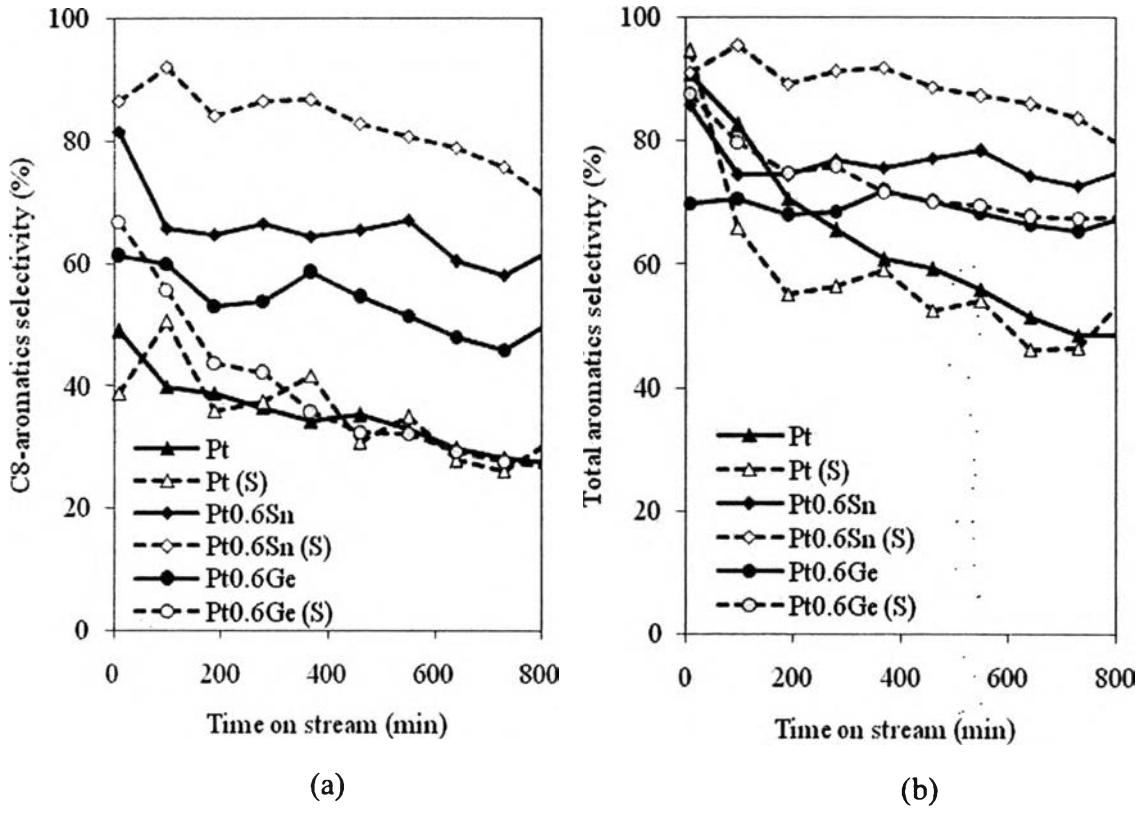

Figure 4.14 The variations of (a) total aromatics selectivity and (b) C8-aromatics selectivity vs. time on stream under 25 ppm sulfur-containing feed over 0.6Pt/KL, 0.6Pt0.6Sn/KL and 0.6Pt0.6Ge/KL catalysts. Reaction conditions: WHSV = 5 h^{-1}; H_2/HC molar ratio = 6; temperature = 500 °C; pressure = 1 atm.

4.3 Characterization of Spent Catalysts

The average particle size of the spent catalysts after reaction under feed containing 25 ppm of sulfur was analyzed by TEM as shown in Figure 4.15. The results showed that in the presence of sulfur poisoning, the particle growth was observed on the unpromoted Pt/KL and promoted PtGe/KL catalysts. In contrast, the Sn-promoted Pt catalyst also exhibited the small particle size of the metals.

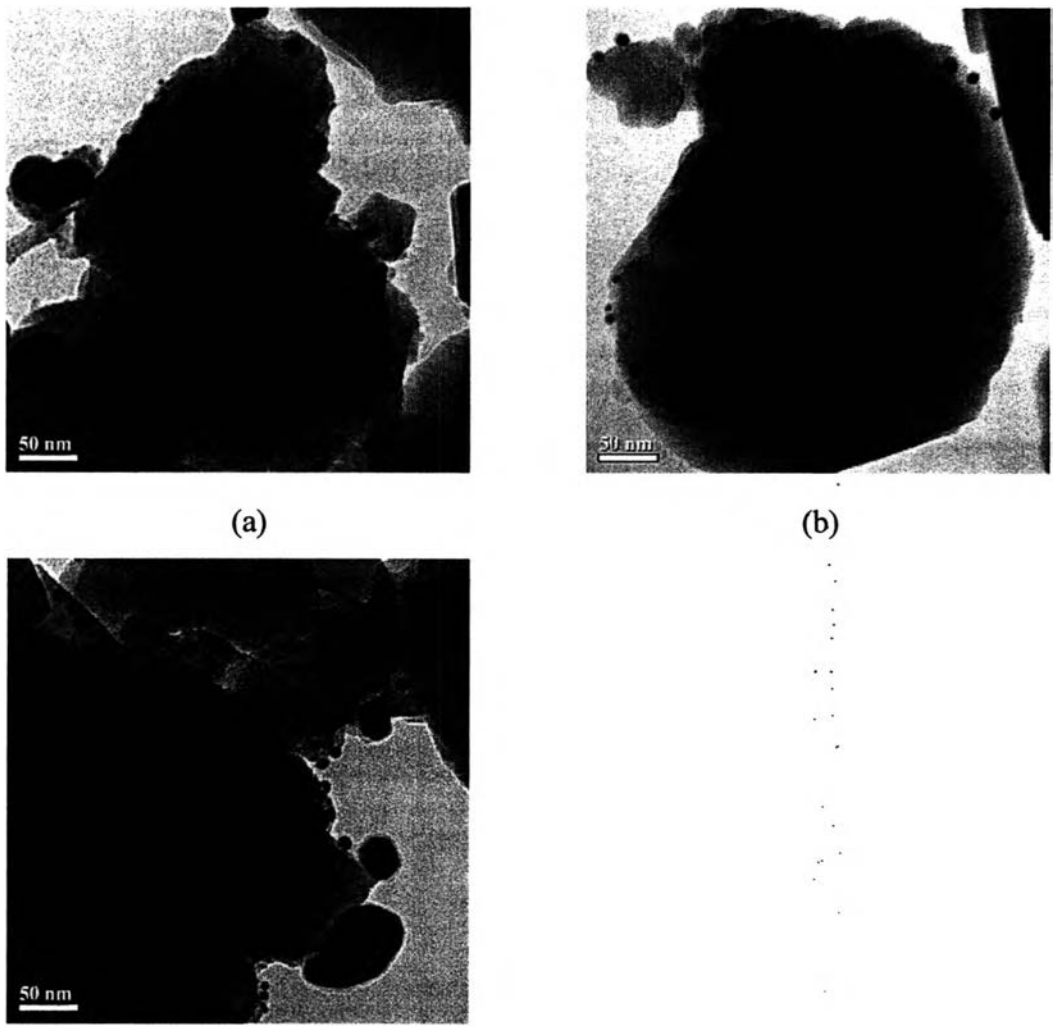

Figure 4.15 TEM images of the monometallic (a) 0.6Pt/KL and bimetallic (b) 0.6Pt0.6Sn/KL and (c) 0.6Pt0.6Ge/KL after reaction under feed containing 25 ppm of sulfur.

The spent catalysts were characterized by TPO to analyze the amount of coke deposited on the catalysts after the reaction in terms of μ mole of carbon/mole of *n*-C8 converted in period of time ratio. The coke formation obtained after reaction under feeds containing sulfur-free and sulfur-containing over Pt/KL, PtSn/KL, and PtGe/KL catalysts are illustrated in Table 4.4.

Table 4.4 TPO analysis of spent Pt/KL, PtSn/KL, and PtGe/KL catalysts under clean and 25 ppm sulfur-containing feed

Catalysts	μ mole of carbon/mole of n-C8 converted in period of time	
	Sulfur-free feed	Sulfur-containing feed
0.6Pt/KL	0.0069	0.0070
0.6Pt0.6Sn/KL	0.0026	0.0022
0.6Pt0.3Ge/KL	0.0067	-
0.6Pt0.6Ge/KL	0.0046	0.0035
0.6Pt1Ge/KL	0.0044	-
0.6Pt3Ge/KL	0.0035	-

The TPO profile obtained after reaction with sulfur-free and sulfur-containing feeds over Pt/KL, PtSn/KL, and PtGe/KL catalysts are illustrated in Figure 4.16. In the case of spent catalysts under clean feed, the monometallic Pt/KL catalyst was deactivated by coke than bimetallic PtSn/KL catalyst. In agreement with the behavior exhibited in the catalytic activity of clean feed, Pt/KL catalyst rapidly deactivated by coke plugging inside the pore of KL zeolite because of the restricted diffusion out of the pore of the C8-aromatic products (EB and OX) (Jongpatiwut *et al.*, 2005). Contrarily, Sn-promoted Pt/KL catalyst have less amount of coke since tin decrease the number of contiguous platinum atoms and then the multipoint adsorption of hydrocarbon molecules on the surface is hampered. Consequently, coke formation can be reduced (Paal *et al.*, 1997). However, the addition of Ge (0.6 wt %) did not decrease in carbon remained on the catalyst. In addition, from TPO profiles described in Figure 4.16, it was found that the bimetallic PtGe/KL catalyst showed some oxidation peak at high temperature. Therefore, it can imply that germanium changes type of coke formation. Besides, the amount of coke deposited decreased when the amount of Ge was in excess (> 0.6 %wt) since the amount of coke precursor was decreased by Ge covering on the active surface area.

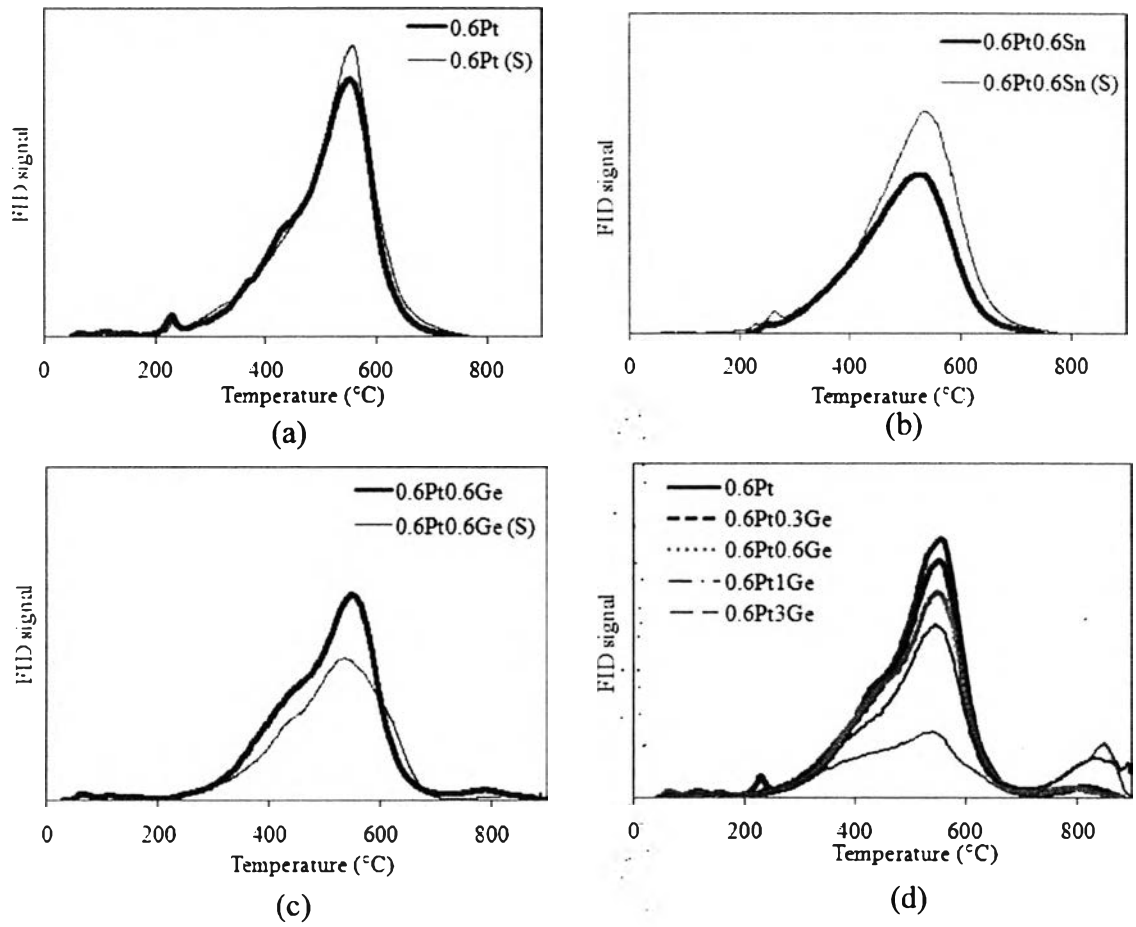

Figure 4.16 TPO profiles of (a) Pt/KL, (b) PtSn/KL, and (c) PtGe/KL catalysts after 810 minutes time on stream under clean and sulfur-containing feeds; and (d) various Ge/Pt ratios of the PtGe/KL catalysts after 810 minutes time on stream under clean feed.

In the case of spent catalysts under sulfur-containing feed, nevertheless, it was noticed that there was no significant change in the amount of coke deposited on the unpromoted Pt/KL catalyst. While, the lower amount of coke deposits produced on the Ge-promoted catalyst as comparing under clean feed. Since sulfur poisoning inhibited the catalytic action of PtGe/KL leading to low formation of coke precursors. On the contrary, after reaction in the presence of sulfur, the Sn-promoted catalyst exhibited a higher activity than those run with sulfur-free feed. Whereas, the ratio of μ mole of carbon/mole of *n*-C8 converted in period of time after reaction in the presence of sulfur was lower than those after reaction in the absence of sulfur.

This exposes that the PtSn/KL in the presence of sulfur induced the decrease of dehydrogenated species, which resulted in carbon deposits as shown in Table 4.3.

To examine the characteristic of catalysts after reaction with sulfur-free and sulfur-containing feeds, the spent catalysts were investigated by TPR after mild decoking at 350 °C for 30 minutes. From figure 4.17, the result displayed that Pt/KL, PtSn/KL, and PtGe/KL catalysts spent with sulfur-free and sulfur-containing feeds lost its structure. However, TPR profile of PtGe/KL catalyst spent with sulfur-containing feed moderately changed position compared with the catalyst spent with sulfur-free feed. This reveals that sulfur persuaded the decrease of Pt-Ge interaction, which resulted in lower conversion as shown in Figure 4.11.

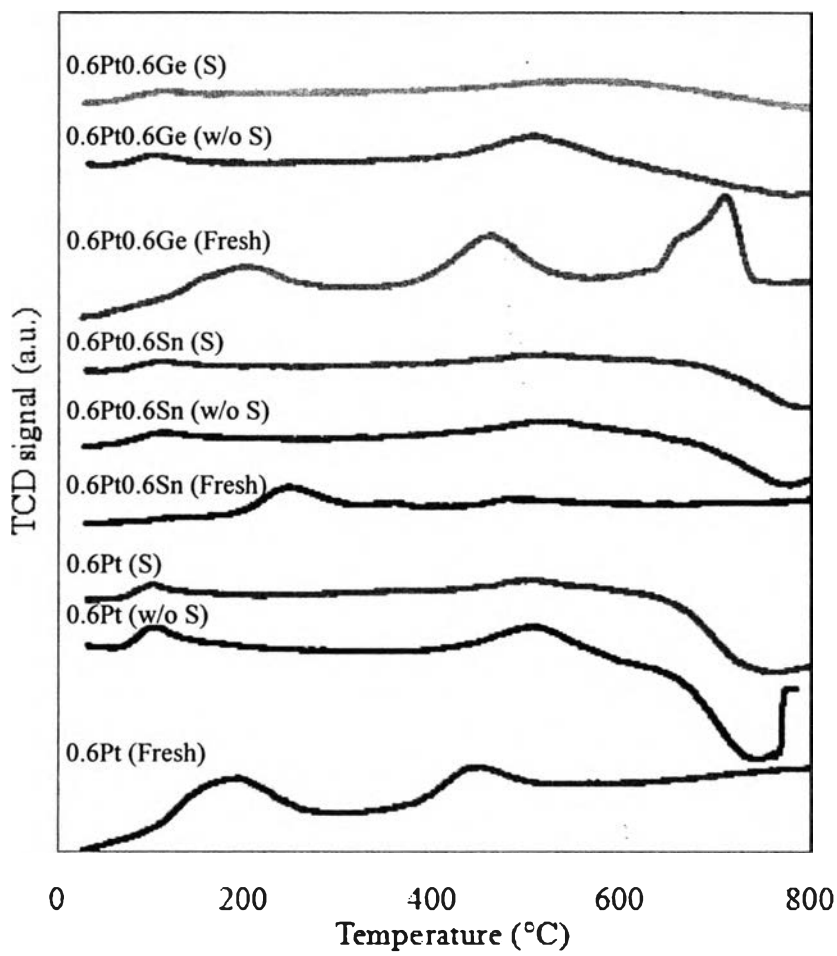

Figure 4.17 TPR profiles of spent Pt/KL, PtSn/KL, and PtGe/KL catalysts under clean and 25 ppm sulfur-containing feeds after mild decoking at 350 °C for 30 minutes.

The characteristic of the catalysts after exposure to reaction in the presence of 25 ppm sulfur was characterize by DRIFTS of adsorbed CO. Figure 4.18 compares the spectra of adsorbed CO on the three catalysts Pt/KL, PtSn/KL, and PtGe/KL before and after reaction with clean and 25 ppm sulfur-containing feed for 810 min. All absorbance of sulfur poisoned catalysts were not different from those of the catalysts spent with clean feed. It could indicate that the Pt surface for stabilized the CO was unaffected by the presence of sulfur.

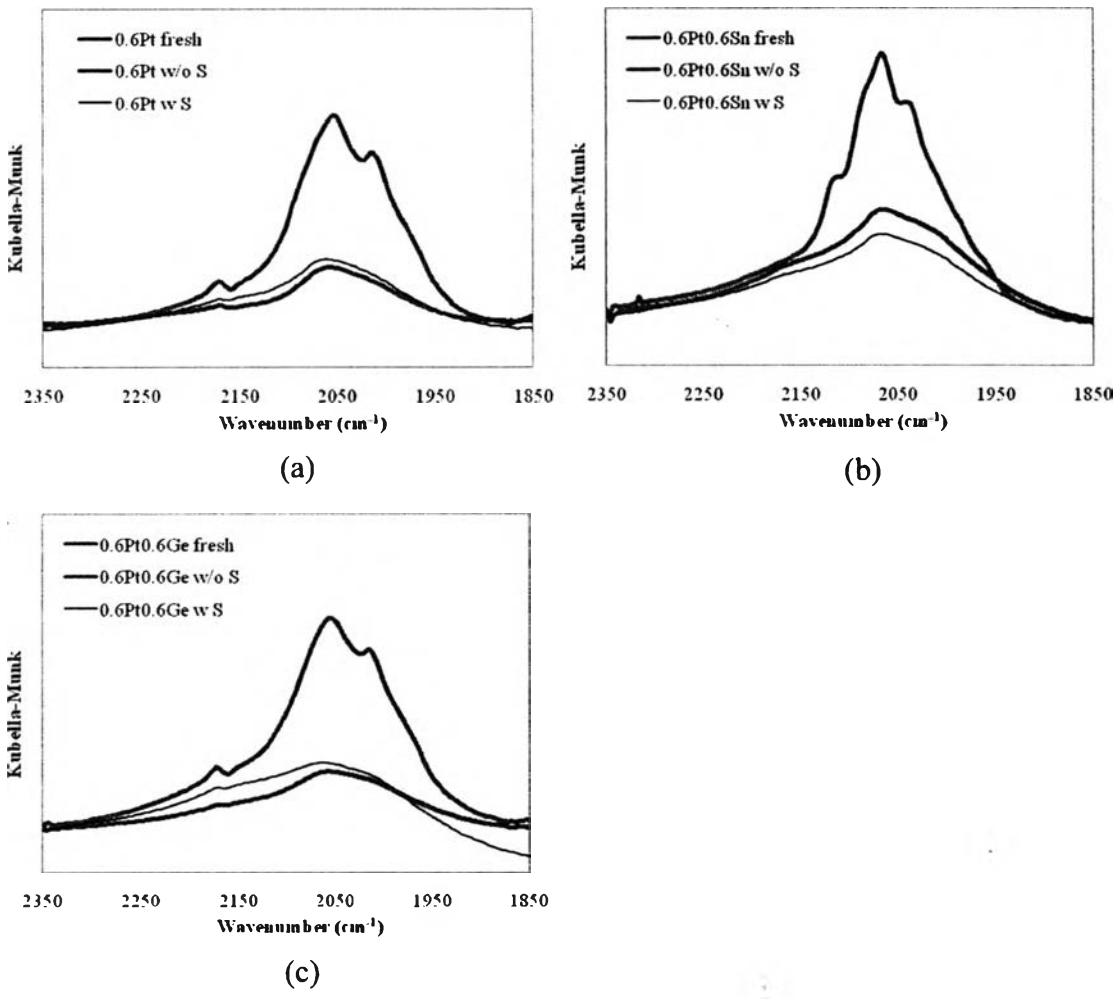

Figure 4.18 DRIFTS spectra of CO adsorbed on (a) Pt/KL, (b) PtSn/KL, and (c) PtGe/KL fresh; after reaction with clean; and 25 ppm sulfur-containing feed for 810 min. Each sample was reduced in situ at 300 °C. The reduced catalysts were exposed to a flow of 3% CO in He for 30 min at 30 °C and purged in He for 30 min.